

Stem cell-derived small extracellular vesicles containing miR-27b-3p attenuated osteoarthritis by targeting leukaemia inhibitory factor expression of synoviocytes

Wei Tong (✉ 2016xh0374@hust.edu.cn)

Wuhan Union Hospital

Xiaoguang Zhang

Wuhan Union Hospital

Wei Chen

the Third Hospital of Hebei Medical University

Shenghui Lan

Xuhui Branch of The Sixth People's Hospital

Yuxiang Hu

Wuhan Union Hospital

Hongxin Pei

Henan Provincial People's Hospital

Zhili He

Wuhan Union Hospital

Zhipeng Dai

Henan Provincial People's Hospital

Yulong Wei

Wuhan Union Hospital

Zhenxing Wang

Wuhan Union Hospital

Qinyu Ma

Third Military Medical University

Fenfei Zhao

Wuhan Institute of Biotechnology

Juan Wang

The Third Hospital of Hebei Medical University

Zengwu Shao

Wuhan Union Hospital

Yong Liu

Wuhan Union Hospital

Shuhua Yang

Wuhan Union Hospital

Hongtao Tian


Wuhan Union Hospital

Article

Keywords:

Posted Date: July 1st, 2022

DOI: <https://doi.org/10.21203/rs.3.rs-1759506/v1>

License:  This work is licensed under a Creative Commons Attribution 4.0 International License.

[Read Full License](#)

Abstract

Mesenchymal stem cell (MSC)-derived small extracellular vesicles (sEVs) have been demonstrated to be effective in the treatment of OA, but the precise target cells and response mechanisms are not well characterised. In this study, first, we found that intra-articular injection of human umbilical cord MSC (UCMSC)-derived sEVs (U-sEVs) significantly alleviated mouse OA. Then, U-sEVs were taken up rapidly and preferentially by fibroblast-like synoviocytes (FLSs) in a mouse model. Furthermore, significant increase in miR-27b-3p in FLSs after U-sEV treatment were found by miRNA sequencing, identifying miR-27b-3p as a key cargo of U-sEVs. Bioinformatics and luciferase reporter found that leukaemia inhibitory factor (LIF) is the target gene of miR-27b-3p, and single-cell RNA-sequencing (scRNA-seq) and RNA-sequencing revealed that LIF could directly induce synovitis, possibly by promoting proinflammatory cytokine and MMPs expression. Lastly, both miR-27b-3p and miR-27b-3p-overexpressing U-sEVs inhibit the expression of LIF in FLSs, and accordingly exhibited stronger effects in mitigating synovitis and OA progression compared to control U-sEVs.

In conclusion, our results revealed that the main recipient cell of U-sEVs in the joints are FLSs. Mechanistically, miR-27b-3p in U-sEVs inhibited LIF expression of FLSs, and thus inhibited synovitis and delayed OA.

Introduction

Osteoarthritis (OA) is the most prevalent degenerative disease of the whole joint, which affects over 355 million people around the world, and is the most common reason for disability in people over 50.¹ It is a highly heterogeneous disease involving the inflammatory injury of all tissues in the joint, including cartilage erosion, synovial inflammation, abnormal remodelling of subchondral bone and ligament injury.² However, the central mechanism of this heterogenous disease is not well delineated and thus no disease-modifying drug has been identified so far.³

Recently, synovial inflammation has been found to play an increasingly important role in OA,⁴ and is reported to be the earliest sign of OA.⁵ In detail, inflammatory synovium releases various inflammatory and chondrocyte catabolic cytokines, such as tumour necrosis factor (TNF), ILs, and MMPs,^{6,7} joint pain and cartilage degeneration. Therefore, pathological change of the synovium is also considered to play a key role in mediating multiple-tissue damage during OA.

In recent years, mesenchymal stem cell (MSC) therapy has shown promising effects in treatment of diseases including OA. Instead of direct tissue-replacement effects,^{8,9,10} increasing studies support indirect effects of these cells, such as by modulating immune responses, and thus enhancing the endogenous repair process. We previously found that umbilical cord MSCs delay OA progression by attenuating synovitis.^{10,11} However, accumulating evidence has shown that MSCs function is mainly via small extracellular vesicles (sEVs).^{12,13,14,15} sEVs are nanosized membrane vesicles (30–200 nm in diameter), which carry various factors including proteins, mRNAs, microRNAs (miRNAs) and so on to

trigger downstream signalling pathways for corresponding therapeutic effect.^{16,17,18} Simultaneously, numerous studies have demonstrated that MSC-derived sEVs with immunomodulatory properties can exert anti-catabolic, anti-inflammatory effects and thus possess cartilage regeneration ability to delay OA.^{17,19,20,21,22} Nonetheless, the precise recipient tissues or cells in the joint, and the underlying response mechanism, remain largely uncharacterised so far.

In this study, we injected human umbilical cord MSCs (UCMSCs)-derived sEVs (U-sEVs) into destabilisation of the medial meniscus (DMM)-induced OA mouse knee joints and found a marked effect in delaying OA progression. Next, we compared the ability of different cells of the joint to take up the U-sEVs and identified that fibroblast-like synoviocytes (FLSs) share the strongest uptake ability of U-sEVs. Furthermore, miRNA sequencing revealed that miR-27b-3p may be a crucial cargo of U-sEVs. Next, by combining RNA sequencing and single-cell RNA-sequencing (scRNA-seq), we revealed that leukaemia inhibitory factor (LIF) is the main target gene of miR-27b-3p in FLSs. Lastly, we found that miR-27b-3p overexpressing U-sEVs exhibited stronger attenuating effects in synovitis and cartilage erosion by inhibiting LIF expression in FLSs.

Results

U-sEVs exhibited comparable effects in delaying OA as USCMCs did

In our previous study, we identified UCMSCs by stem cell markers.²³ Then UCMSC-derived small extracellular vesicles (U-sEVs) were successfully isolated and characterised by TEM, dynamic light scattering (DLS), and western blotting.²⁴ Further nanoparticle tracking analysis (NTA) by DLS demonstrated that the diameter of particles ranged from 30 to 200 nm and contained U-sEVs (Figure S1A). The cup-shaped morphology of sEVs was revealed by TEM (Figure S1B). Lastly, western blotting revealed that sEV-specific surface markers (ALIX, CD63, CD81, CD9) were expressed on U-sEVs and negative protein (Calnexin) was more highly expressed on cells (Figure S1C).

We next studied the effect of UCMSCs and U-sEVs on OA induced by DMM in mice (Fig. 1A). Eight weeks after surgery, mouse knees displayed a typical OA phenotype: less safranin-O staining, fibrillation at the cartilage surface, and cartilage clefts (Fig. 1B). In contrast, these phenotypic changes were partially but significantly attenuated by U-sEV, similar to direct UCMSCs treatment (Fig. 1B). Consistent with this, Mankin scores and OARSI grade demonstrated that U-sEVs produced a 36.2% and 40.7% decrease compared with control (Fig. 1E). The reductions in the uncalcified zone, calcified zone, the percentage of uncalcified zone of articular cartilage and total cartilage thickness were all significantly salvaged by U-sEVs compared with vehicle treated DMM mice (Fig. 1F). Radiological focal defects and osteophyte formation around the knee joint were detected by micro-CT (Fig. 1C), and both UCMSC and U-sEV groups showed a lower OA grade compared to the DMM group (Fig. 1D). Furthermore, MMP-13 and ADAMTS-5

which are markers of chondrocytes catabolism and degraded cartilage matrix, were reduced by treatment with UCMSCs and U-sEVs compared with the DMM control group (Fig. 1G, H).

Synovitis is an independent aetiology of OA and the main cause of joint pain, which is characterised by synovial hyperplasia and inflammatory cell infiltration. H&E staining showed that obvious inflammatory cell infiltration and hyperplasia in DMM synovium were alleviated by treatment with UCMSCs and U-sEVs (Fig. 1I, J). Furthermore, von Frey assay was performed to evaluate joint pain of OA mice and revealed that U-sEVs alleviated the decline of the paw withdrawal threshold (PWT) in the early and middle stages post treatment compared with the DMM group, with UCMSCs being more effective (Fig. 1K).

Taken together, these data demonstrated that U-sEVs significantly delayed OA progression, recapitulating the effects of direct UCMSC introduction to quite a high level.

FLSs are the main recipient cells of U-sEVs

As OA is a highly heterogenous disease involving multiple tissues of the whole joint, we next tried to identify the main tissues and cells responding to the U-sEVs. We first compared the distribution of U-sEVs *in vivo*. U-sEVs fluorescently labeled with DiO dye (green) were injected into mouse knee joints after DMM and revealed that U-sEVs were mainly distributed in the synovium, gradually migrating from the surface to the deep layer from day 1 to day 7 (Fig. 2A). In addition, a moderate number of U-sEVs could also be observed at the superficial layer of the cartilage, while some could be seen in the deep layer at day 7 (Fig. 2B). However, very few U-sEVs were distributed in the meniscus (Fig. 2C).

As U-sEVs were mainly distributed in synovium and cartilage, we further explored the specific responding cells within those tissues by comparing the uptake ability of FLSs, chondrocytes (CHOs), meniscus fibrochondrocytes (MFCs), and also macrophages which are the main cause of synovitis. FLSs, CHOs, MFCs and inflammation induced RAW 264.7 macrophage cells (Figure S2A), were incubated with DiO-labeled U-sEVs *in vitro*. After 30 min, 1 hour and 2 hours, immunofluorescence showed that green signals were most enriched in FLSs. Conversely, CHO and MFCs engulfed significantly fewer U-sEVs (Fig. 2D-G). Mean fluorescent intensity (MFI) per cell also indicated consistent result (Fig. 2G). As macrophage infiltration contributed greatly to synovitis as well, we compared the uptake of sEVs between FLSs and macrophages and found that macrophages did not take up as many sEVs as FLSs (Figure S2B, C).

In summary, U-sEVs were mostly distributed in the synovium, and FLSs were the main responding cells of U-sEVs, responsible for the effects of U-sEVs on OA.

MiR-27b-3p was an important cargo of U-sEVs and could inhibit LIF expression in FLSs to alleviate synovitis in OA

To further understand the molecular mechanism of U-sEVs on synovium, mouse FLSs were first treated with IL-1 β to induce inflammation and then incubated with U-sEVs or vehicle for 2 h. Then, RNA was

extracted for both mRNA and miRNA sequencing as miRNAs were considered to be the functional component of EVs.

The significantly differentially enriched miRNAs in FLSs were displayed as a heatmap (Fig. 3A), which showed that miR-155-5p, miR-223-3p, miR-760, miR-142-3p, miR-27b-3p and let-7i-5p were evidently upregulated when FLSs took up U-sEVs (Fig. 3B). Those miRNAs regulated downstream genes associated with inflammation, angiogenesis-related functions, and extracellular matrix (ECM) catabolic enzymes (MMPs and ADAMTS) (Figure S3A, B), indicating inhibitory effects of U-sEVs in FLS mediated inflammation and cartilage erosion. Interestingly, U-sEVs markedly decreased the expression of TNF signalling pathway, NF- κ B signalling pathway, and inflammatory response-, ECM and angiogenesis related genes in FLS (Figure S3C, D).

To identify the specific and most functional miRNAs, the top 40 high-abundance miRNAs in U-sEVs were picked up according to transcripts per million reads (TPM) and revealed that miR-27b-3p was the most enriched miRNA in U-sEVs (Fig. 3C), indicating a dominant role of miR-27b-3p (Fig. 3D). Moreover, volcano plots showed that the amount of miR-27b-3p among differentially varied miRNA was increased in FLSs (Fig. 3E), which was corroborated by RT-PCR assay of FLSs (Fig. 3F). Therefore, these results strongly suggested that miR-27b-3p was the most enriched miRNA in U-sEVs and was also significantly internalised by FLSs after treatment. To validate the function of miR-27b-3p in OA, we transfected miR-27b-3p antagomir, miR-27b-3p agomir and their negative control (NC) respectively into mice knee joints and harvested the joints for analysis 8 weeks after DMM surgery. Compared with NC treatment, we found that miR-27b-3p antagomir induced more severe synovitis, while miR-27b-3p agomir could greatly attenuate this phenotype (Fig. 3G, H).

We next explored the specific target gene of miR-27b-3p in FLS. The miRWalk, miRDB and Targetscan databases were used to identify putative targets, and the NCBI database was used to restrict the range to synovitis-related genes, which identified 31 genes to be the target genes of miR-27b-3p (Fig. 3I, S4A). Notably, Leukaemia inhibitory factor (LIF), a member of the interleukin (IL)-6 cytokine superfamily,²⁵ one of the genes significantly down-regulated by U-sEV treatment (Figure S3E, H), was also a target gene of miR-27b-3p (Figure S4B). Conversely, a Venn diagram presenting information of TPM, Targetscan, miRDB and miRwalk (Figure S3I) prescribed a limit of 28 miRNAs as possible upstream miRNAs targeting LIF, which also contained miR-27b-3p (Figure S4C). To verify the effects of miR-27b-3p on LIF, mouse FLSs were transfected with miR-27b-3p mimic oligonucleotides (miR-27b-3p mimics) and negative control oligonucleotides (mimics NC). RT-PCR, western blotting and immunofluorescence demonstrated that miR-27b-3p decreased the expression of LIF in mouse FLSs (Fig. 3J, K, L). To validate the direct binding of miR-27b-3p to LIF, luciferase reporter assay analysis was performed, and confirmed that LIF was the downstream target of miR-27b-3p (Figure S5A, B). Taken together, these data strongly suggested that miR-27b-3p was the functional cargo of U-sEV which inhibited LIF expression in FLSs.

MiR-27b-3p was the functional cargo of U-sEVs to modulate synovitis by inhibiting LIF in FLSs

To validate the function of LIF on synovitis, we injected recombinant human LIF protein (rhLIF) into mouse knee joints and euthanised the mice four weeks later for histological observation. The synovium of rhLIF-treated knees appeared thicker and had a higher score (100% increase, $P < 0.01$) compared to vehicle-treated ones (Fig. 4A, B). Immunofluorescence indicated that rhLIF enhanced the production of IL-6 (Fig. 4C), a key product of LIF pathway and OA pathogenic factor. Moreover, IL-6 expression in mouse FLSs was obviously increased by rhLIF (Fig. 4D, E, F). On the contrary, inhibition of LIF by injecting methoxy modified LIF siRNA (m-si*LIF*) into OA knees significantly attenuated LIF expression in synovium (Fig. 4G), along with the alleviation of synovitis (Fig. 4H, I). Other proinflammatory factors and ECM catabolic factors such as CCL3, CXCL1 and MMP-1, were downregulated in si*LIF* transfected mouse FLSs compared to negative control (si*LIF* NC) (Fig. 4J, K). These data obviously indicated the important role of LIF in synovitis.

To explore the regulatory effects of LIF on macrophage migration, we seeded FLSs into the lower chamber of each well and induced them with rhLIF and IL-1 β respectively, and inflammation-induced RAW 264.7 macrophage cells were seeded into the upper chamber of transwell filters. Crystal violet staining showed that rhLIF treated FLS could enhance macrophage migration. Moreover, inflamed FLS could significantly induce macrophage migration, which was substantially blocked by si*LIF*, which indicated that migration of macrophage is LIF dependent. (Fig. 4L, M). However, we did not see a direct effect of rhLIF on macrophage migration (Figure S6A, B), possibly due to that LIF receptor subunit alpha (LIFR) was not enriched in monocyte-macrophage lineage cells according but in FLSs by scRNA sequencing (Figure S6 C, D). These data demonstrated that LIF could indirectly stimulate macrophage infiltration through FLSs.

In conclusion, we found a positive association between LIF expression in FLSs and synovitis, and also validated the function of LIF in synovial inflammation in mouse possibly by promoting proinflammatory cytokine secretion and thus enhanced macrophages infiltration occurred.

MiR-27b-3p in U-sEVs downregulated LIF expression in FLSs and thus alleviated synovitis

As we hypothesised that miR-27b-3p was a crucial cargo in the action of sEVs on synovitis possibly by inhibiting LIF, we generated miR-27b-3p-overexpressing U-sEVs (U-sEV^{miR-27b-3p}) (Figure S7A) and explored its effects and mechanism. After repeated injection as scheduled (Fig. 1A), we found that the remission effect of U-sEV^{miR-27b-3p} on synovitis was more marked than that of U-sEV^{NC}, exhibited as a reduction in synovial hyperplasia, lower score and less pain (Fig. 5A, B, C). Moreover, CD14⁺ and CD68⁺ macrophage infiltration and angiogenesis²⁶ of the synovium both contributed greatly to synovitis, and were greatly attenuated by U-sEV^{NC} especially U-sEV^{miR-27b-3p} according to immunofluorescence data (Fig. 5D), and were strongly associated with modulation of LIF expression (Fig. 5E, S7B-E).

To further explore the effects of miR-27b-3p on LIF expression in FLS, we carried out cell culture experiments. U-sEVs were isolated from UCMSCs treated either with miR-27b-3p neutralising

oligonucleotide (U-sEV^{anti-miR-27b-3p}) or a control oligonucleotide sequence (U-sEV^{anti-NC}) and then incubated with IL-1 β -induced FLSs. The expression of LIF in U-sEV^{anti-miR-27b-3p}-treated FLSs was higher than in FLSs treated with U-sEV^{anti-NC}, while U-sEV^{miR-27b-3p} markedly reduced LIF expression as compared to U-sEV^{NC}, and IL-6 accordingly (Fig. 5F, G). In line with this, miR-27b-3p mimics inhibited LIF expression of FLS as well as other LIF-induced cytokines such as IL-6, CXCL1, and CCL3, while miR-27b-3p inhibitor exhibited opposite effects and their control oligonucleotides. The expression of LIF and other LIF-induced cytokines such as IL-6, CXCL1, and CCL3 were also markedly reduced (Figure S8A, B).

To delineate the function of LIF and how miR-27b-3p in U-sEVs modulate LIF function, we incubated FLSs with rhLIF, and then treated with U-sEV^{NC} or U-sEV^{miR-27b-3p}. The results showed that the expression level of LIF, IL-6 and other inflammatory factors (CCL3 and CXCL1) that played an important role in synovitis were activated by rhLIF, and could be rescued by U-sEV^{NC} and especially by U-sEV^{miR-27b-3p} (Fig. 5H, I). Therefore, abnormally high LIF induced multiple proinflammatory cytokine secretion of FLS, which was substantially abolished by miR-27b-3p of U-sEVs.

As those proinflammatory cytokine could induce macrophage infiltration, a key phenotype in OA synovitis, we further explored the regulatory effects of miR-27b-3p in U-sEVs on macrophage migration. We induced inflammation in RAW 264.7 macrophage cells and seeded them into the upper chamber of transwell filters, while FLSs were seeded into the lower chamber of each well. Crystal violet staining showed that rhLIF enhanced the migration of macrophages, which was blocked by U-sEV^{NC} and especially U-sEV^{miR-27b-3p} (Fig. 5J, K). Those data suggested that miR-27b-3p in U-sEVs inhibited macrophage infiltration by inhibiting LIF expression during synovitis.

Taken together, we strongly suggested that miR-27b-3p was a key cargo in U-sEVs to inhibit LIF expression of FLS, which mitigated macrophage migration and synovitis.

LIF expression in FLSs was strongly associated with synovial inflammation of OA patients by single-cell RNA sequencing

To increase the clinical significance of our study, we explored the association of LIF in synovitis of OA patients. We first harvested synovium from both healthy and late stage OA patients' knees who need total knee arthroplasty, and synovitis in OA was confirmed by H&E staining as hyperplasia and inflammatory cell infiltration (Fig. 6A), which was in line with a previous study.²⁷ Later, a single cell suspension of 1×10^4 cells was prepared for single-cell RNA sequencing (scRNA-seq) (Fig. 6B). To analyse the scRNA-seq data, the barcoded transcripts from each single cell were counted and transcript expression from all individual cells yielded eight major clusters (Fig. 6C). Uniform manifold approximation and projection (UMAP) including all individual cells from two samples confirmed the presence of eight distinct single cell clusters: monocyte-macrophage lineage cells, fibroblast-like synoviocytes (FLSs, including synovial lining

FLSs and synovial sublining FLSs), T /NK cells, myocytes, mast cells, endothelial cells and plasmablasts (Fig. 6D, S9A). FLSs, including both lining and sub-lining FLS, contributed to the largest portion of total synovial cells (49.3%) (Figure S9B), and therefore possibly played key roles in synovitis.

In order to predict the difference in gene function of FLS, KEGG and GO analysis were performed. KEGG pathway enrichment showed that, compared with normal synovium, inflammation- and immune-related pathways in OA synovium including “NF-kappa B signalling pathway”, “TNF signalling pathway”, “Rheumatoid arthritis”, and “IL-17 signalling pathway” were upregulated in the FLS cluster (Figure S9C). Similarly, GO analysis showed that inflammation-related functional genes such as “leukocyte cell – cell adhesion” and “response to interleukin – 1” were upregulated in the FLSs cluster (Figure S9D). To further decipher whether these increased transcripts of genes between the two groups were related to inflammation, we performed gene set enrichment analysis (GSEA) using KEGG and GO gene sets and found that “TNF signalling pathway” ($P = 0.014534$), “NF-kappa B signalling pathway” ($P = 1.83 \times 10^{-5}$), “regulation of leukocyte mediated immunity” and so on were strongly enriched in OA synovium ($P = 0.003496$) (Figure S10), which provided strong evidence of inflammatory reaction in OA synovium.

Based on the above conclusions, we next performed real-time PCR of normal and OA synovium, and identified the most significantly ($P < 0.05$) up-regulated genes derived from the above pathways (Figure S9C, D) in synovial fibroblasts. Among them, LIF were the third differentially-expressed genes (Fig. 6E), which increased mainly in FLS cluster (Fig. 6F, G). Furthermore, IHC staining showed that LIF was more enriched in the synovium of DMM-induced mice compare to sham (Figure S11), indicating a critical role of FLSs derived LIF in OA. Those data further indicated a strong positive association of FLSs expressed LIF with synovial inflammation in OA patients.

Discussion

Numerous studies have shown promising effects of EVs on OA. However, unlike stem cells, there has been no clinical trial of EVs in OA, possibly due to the large cell numbers needed and the reliable quality to generate enough homogenous EVs.²⁸ Moreover, few studies explored the precise recipient tissue or cells of EVs after injection, nor the subsequent response mechanism to identify the key target. In this study, we generated sEVs from good manufacturing practice (GMP) grade UCMSCs, in an effort to guarantee the cell quantity and quality, which is vital for the homogeneity of U-sEVs,²⁴ and therefore paved the way for rapid clinical application in the near future. Secondly, this study compared the uptake ability of cells in the joint, and identified that U-sEVs were taken up rapidly and preferentially by FLS, possibly due to the fact that those cells share very high cholesterol biosynthesis,²⁹ which is vital for EVs uptake and subsequent signal transduction.^{30,31} This finding provided insight for the more feasible generation of engineered EVs to target accurate cells and thus exhibit stronger effects. Thirdly, through a combination of sequencing from tissue level to single cell resolution, we identified that LIF played a key role in synovitis and OA.

Multiple stem cells including tissue-specific MSCs, iPSCs and so on are used for tissue regeneration and disease treatment, and sEVs from these stem cells have also been shown to be effective in animal models of various diseases such as myocardial infarction, inflammatory pulmonary disease and OA.^{32,33,34} However, numerous factors such as FBS in the media, differences in cell passage number, isolation method and so on influence the quality and quantity of EVs,³⁵ so ISEV has issued standard guidelines trying to generate high-quality EVs.²⁴ GMP-grade cells have the advantage for EV production: the large numbers of cells in GMP grade facilities, strict quality control of cells before use and so on,³⁶ so as to ensure high EV yield and rapid clinical application.^{33,36} In our study, we generated sEVs from GMP-grade UCMSCs, which we are now employing in a clinical trial on OA patients (ChiCTR2000039017, <http://www.chictr.org.cn/showproj.aspx?proj=62498>). sEVs from the GMP-grade UCMSCs almost mimicked the effects of direct UCMSC injection on OA, significantly attenuating OA progression (Fig. 1B-F). In addition, different stem cells each have their own advantages in different tissue regeneration and disease treatment approaches, so comparisons between EVs from different stem cells are interesting.

sEVs carry molecules including proteins, lipids, RNA and DNA to deliver information between cells,³⁷ and several studies consider miRNA in EVs as the main functional cargo responsible for their effects.^{38,39} In OA field, miRNAs including miR-100-5p⁴⁰ and miR-26a-5p⁴¹ from different stem cell-derived sEVs enhance cartilage regeneration.^{42,43,44,45,46,47,48} Nonetheless, no study has identified the exact recipient cell and its responding mechanism. In this study, the uptake assay showed that FLSs owned the strongest uptake ability of U-sEVs (Fig. 2). Based on this, we next performed miRNA sequencing of U-sEVs before and after FLS incubation, and coincidentally found that miR-27b-3p was the most abundant and among the most differentially changed miRNA in U-sEVs, which comprehensively implicated miR-27b-3p as an important cargo for U-sEV function. To validate this, miR-27b-3p-overexpressing U-sEVs were generated and found to significantly attenuate FLSs-mediated synovitis by inhibiting macrophage infiltration. In agreement with our findings, miR-27b-3p has been shown to delay OA progression by targeting TNF receptor-associated factor 3 (TRAF3),⁴⁹ indicating a positive role of miR-27b-3p in delaying OA by targeting multiple downstream genes of different cells, a typical functional pattern of miR-mRNA interaction.⁴⁶ Regarding our study, the mRNA sequencing of U-sEVs-treated FLSs demonstrated that LIF was one significant target gene of miR-27b-3p in these cells (Fig. 3).

LIF, as a member of the interleukin-6 family, is one of the downstream genes of the NF-kappa B signalling pathway⁵⁰ and associated with many inflammatory diseases.^{51,52} The downstream signalling pathway of LIF is similar to that of Oncostatin M (LIFR/gp130- Jak- STAT),⁵³ another IL-6 family cytokine, which contributes greatly to synovial fibroblast-mediated synovitis and joint destruction in arthritis.⁵⁴ Notably, previous studies showed that LIF is expressed in cartilage and synovium and contributes to the pathogenesis of arthritis,⁵⁵ and tissue levels of LIF varies depending on the osteoarthritis grade.⁵⁶ However, no study has exactly delineated the effect of LIF in synovitis and OA. In this study, we identified upregulation of both the NF-kB pathway and LIF in mouse and human synovium (Figure S9, 6E-G), indicating a strong association between the NF-kB /LIF pathway in OA synovitis. Furthermore, rhLIF

upregulated expression of proinflammatory factors, such as expression of IL-6, CXCL-1, and CCL3, and modulates macrophage migration (Fig. 4J, K, 5H, I). Therefore, LIF alone could induce synovitis, and become a potential therapeutic target of OA.

Fibroblast-like synoviocytes (FLSs) reside in both the lining and sub-lining layer of the synovium, and contribute directly to inflammation by secreting proinflammatory cytokines such as ILs, CCLs, and CXCLs,^{57,58} as well as MMPs and ADAMTSs to degrade cartilage and subchondral bone. In our study, by scRNA-seq of both healthy and OA patients, we found that several cytokines including LIF were significantly upregulated in OA synovium compared to normal synovium and were mostly enriched in lining FLSs (Fig. 6). In addition, LIF inhibition greatly attenuated macrophage infiltration, which reported to be the main infiltrating inflammatory cells in synovitis. However, LIF had almost no direct effect on macrophage migration, possibly due to low level of LIFR expression in monocyte-macrophage lineage cells (Figure S6), so our study identified a new mechanism for FLS-macrophage crosstalk-mediated synovitis. However, two distinct subtypes of FLSs played selective roles in cartilage-bone destruction (sublining layer FLSs) and joint inflammation (lining layer FLSs) in RA patients,⁵⁹ so further study to deeply explore individual function of those two subpopulations in OA is necessary.

There are several limitations to this study. First, we found that LIF is the main targeted gene of U-sEVs in FLSs, so a tissue-specific knockout animal model, such as LIF-specific deletion in FLSs by using Col-6a1-Cre mice,⁶⁰ is needed to accurately validate the function of LIF in various cells. Secondly, single-cell analysis on synovium before and after U-sEV treatment to compare the cell cluster and specific gene changes at single-cell resolution could help strengthen our conclusions. Lastly, dynamic changes of joint mechanics, hormone level in human is highly associated with OA progression, so a nonhuman primate model, which could better mimic human physiology than a rodent model,⁶¹ is needed to solidly validate the function of U-sEVs.

Conclusions

In summary, we compared the uptake ability of multiple cells in the joint, and identified that FLSs shared the strongest ability to ingest U-sEVs. After a serial sequencing and both *in vitro* and *in vivo* experiments, we demonstrated that GMP-grade U-sEVs have the potential to attenuate OA progression by inhibiting LIF expression in FLS via miR-27b-3p to alleviate synovitis and thus OA (Fig. 7). Our study may lead to provision of promising clinically-available sEVs for OA treatment.

Materials And Methods

Preparation of human UCMSCs and isolation of U-sEVs

Good manufacturing practice (GMP) grade UCMSCs were obtained from Wuhan Hamilton Biotechnology Co., Ltd., Wuhan, China, and cultured in special growth medium (Human Umbilical Cord Mesenchymal Stem Cells Serum-Free Basal Medium Cat. No. HUXUC-03061) containing 100 µg/mL penicillin and 100

U/mL streptomycin (P/S) at 37°C in 5% CO₂. The medium was changed twice a week. Cells were passaged when 90% confluence was reached, and at passage 4–8 were used for experiments.

After culture to 80% density on 10 cm cell culture dishes, UCMSCs were washed with phosphate-buffered saline (PBS) for sEV preparation. The medium was then replaced with StemXVivo serum-free human MSC expansion medium (CCM014, R&D systems, Minneapolis, MN, USA) containing 10% EV-depleted foetal bovine serum (FBS) (C3801-0050, VivaCell Biotechnology GmbH, Denzlingen, Germany), 1% sodium pyruvate (S/P), 1% L-glutamine (L-Glu) and 1% P/S. After culture for 48 h, the UCMSC-conditioned medium (CM) was collected and centrifuged at 3000 × *g* for 15 min then at 10,000 × *g* for 30 min, and was then passed through a 0.22-µm filter to completely remove impurities and cellular debris. For sEV preparation, the supernatant was ultracentrifuged for 70 min at 110,000 × *g* and was aspirated. The remaining pellets were resuspended in PBS and centrifuged for 70 min at 110,000 × *g* once more. The resulting pellets, which contained the isolated sEVs, were resuspended in PBS for further experiments. All purification steps were performed at 4°C and followed the purification protocol described previously.⁶² Protein concentrations of isolated sEVs were measured using a Pierce Microplate BCA Protein Assay Kit (23252, Thermo Fisher Scientific, Waltham, MA, USA) and a spectrophotometer (Bio-Tek, Winooski, VT, USA). A total of 10 µg of U-sEVs could be extracted from every 20 mL of medium.

Characterisation of U-EVs

A transmission electron microscope (Tecnai F20 FEI 200KV) was used to visualise the U-sEVs. After fixation with 3% glutaraldehyde for 2 h and negative staining with uranyl acetate for 15 min, U-sEVs were centrifuged at 13,000 × *g* for 3 min. Next, the U-sEVs were resuspended, dehydrated in absolute ethanol for 10 min and loaded onto copper grids before immersing in 1% phosphotungstic acid to contrast the grids and then washing the grids several times using absolute ethanol. The samples on grids were frozen in liquid nitrogen and analysed by transmission electron microscopy (TEM).

The size of U-sEVs was measured by dynamic light scattering (DLS) using a NanoSight LM10-12 (Malvern Panalytical, Malvern, UK). Isolated U-sEVs were resuspended in PBS and loaded into a UV-transparent cuvette. Particle size measurement was repeated at least three times by different independent persons. Nanoparticle tracking analysis (NTA) was performed to obtain size distribution and particle concentration of sEVs using software provided by the manufacturer (NTA 3.1 build 3.1.54; Malvern Panalytical). After dilution in PBS at concentrations from 1:10 to 1:100, samples were treated to obtain a corresponding concentration within the recommended measurement range (20–30 particles/frame). A 60 s video of dynamic particles was recorded by the software at a temperature between 20 and 23°C. Approximately 10 µg of sample produced 1 × 10⁹ U-sEVs on average, derived from 20 mL CM, according to the outcome of NTA in this study. Each value was the mean of three individual measurements.

Isolation of mouse FLSs, chondrocyts (CHO) and meniscus fibroblast chondrocytes (MFCs) and preparation of murine

RAW 264.7 macrophage cells

The bone-end cartilage of 3-day-old mouse pups and the meniscus of mature mice were cut off and digested with 0.25% trypsin (Invitrogen, Carlsbad, CA, USA) for 30 min, and were further digested with 173 U/mL collagenase Type I (Worthington Biochemical Corporation, Lakewood, NJ, USA) for 4 h. Undigested tissues were removed by filtration. The cells in the supernatant were centrifuged and resuspended in Dulbecco's Modified Eagle Medium (DMEM) containing 15% FBS, 100 µg/mL streptomycin and 100 U/mL penicillin and cultured at 37°C in 5% CO₂, and attached cells were considered to be primary CHOs or MFCs.

After euthanising mice, the synovium tissue was dissected and digested with 0.2% collagenase Type 2 (Sigma–Aldrich, St Louis, MO, USA) for 6 h, followed by digestion with 0.25% trypsin–EDTA for 30 min. After filtration and centrifugation, the remaining cells were considered to be primary FLSs and cultured.

RAW 264.7 cells (Bioswamp Life Science Lab. Co., Ltd, Hubei, China; CELL-C0190) were used to mimic and substitute for macrophages *in vitro*.

After culture of RAW 264.7 macrophages in growth medium (DMEM containing 15% FBS), the medium was replaced with activation medium containing 1 mg/mL lipopolysaccharide (LPS, Solarbio, Beijing, China; L8880). After 24 h of induction, cells were deemed to be activated macrophages.^{63,64}

U-sEV internalisation in vitro and in vivo

U-sEVs were labeled with DiO (Invitrogen) membrane dye following the manufacturer's protocol. Briefly, U-sEVs were incubated with 1 µmol/L DiO for 5 min, then ultracentrifuged to remove excess dye at 100,000 × *g* for 70 min. After washing three times, the green fluorescence-labeled U-sEVs finally obtained were re-suspended in PBS, then 5 × 10⁸ particles/mL of labeled U-sEVs were cultured with FLSs, CHOs, MFCs or RAW 264.7 macrophages. After 30 min, 1 h or 2 h of culture, cells were washed with PBS and fixed in 4% paraformaldehyde, then stained with phalloidin (AAT Bioquest, Sunnyvale, CA, USA) and DAPI. The uptake of U-sEVs *in vitro* was observed using a confocal microscope.

To observe the uptake of U-sEVs in the mouse knee joint cavity, intra-articular injection with green fluorescence-labeled U-sEVs (1 × 10⁸ particles)¹⁹ was performed. After 24 or 48 h, mice were euthanised, their knee joints were removed, and frozen sections were prepared. After staining with DAPI, frozen sections were observed using a confocal microscope.

Animals

Male C57BL/6 mice were used as experimental animals which were purchased from the animal experimental centre of Huazhong University of Science and Technology (Wuhan, Hubei, China). The Animal Care and Use Committee of Union Hospital, Huazhong University of Science and Technology approved all animal experiments related to this study which were also consistent with the Animal Welfare

Act in accordance with the Standing Committee on Ethics in China (State Scientific and Technological Commission of China).

OA induction and treatment: Male C57BL/6 mice were group-raised in ventilated cages, and cotton pads were changed once every 2 days until they reached 12 weeks of age and were used for animal experiments. After anaesthesia with 2% isoflurane, mice underwent unilateral (left) DMM surgery by transection of the tibial ligament of the medial meniscus.⁶⁵ The remaining eight mice underwent sham surgery as the normal control group. Mouse joints were injected with free UCMSCs (3×10^4 cells in 5 μ L PBS) and U-sEVs (1×10^9 particles in 5 μ L PBS) using a microliter syringe (Hamilton Company, Reno, NV, USA; 1702) and 5 mm 30-gauge needles (Hamilton Company; 7803–05) at 0, 2 and 4 weeks after DMM surgery. Meanwhile, animals in the U-sEV^{NC} and U-sEV^{miR-27b-3p} groups were treated with miR-27b-3p-overexpressing U-sEVs (U-sEV^{miR-27b-3p}) and negative control U-sEVs (U-sEV^{NC}) respectively. Animals in the rhLIF group were treated with 0.2 mg/mL rhLIF (L5283, Sigma-Aldrich) protein in 5 μ L PBS. All experimental mice were euthanised 8 weeks after surgery for further histological analysis.

To further verify the effect of miR-27b-3p, thirty mice were randomly assigned to the following five groups consisting of six mice per group: (1) Sham; (2) DMM + antagomir NC (30 μ g in 50 μ l) (GenePharma Co. Ltd., Shanghai, China); (3) DMM + miR-27b-3p antagomir; (4) DMM + agomir NC; (5) DMM + miR-27b-3p agomir. Treated mice were euthanised 4 weeks after surgery for further histological analysis.

Histology

After immersion in 4% paraformaldehyde overnight, harvested knee joints were decalcified in 15% EDTA for 4 weeks followed by dehydration in a graded series of ethanol (from 75–95%) before paraffin embedding. A microtome was used to cut the paraffin-embedded samples into continuous 7- μ m-thick sections from the medial side to the cruciate ligament junction. The remaining half samples were made into frozen sections. After being decalcified in 15% EDTA for 2 days, frozen samples were treated with 15% sucrose with 2% polyvinylpyrrolidone (PVP) and then frozen in 8% gelatine. Finally, they were continuously sectioned at a thickness of 30 μ m.

The first batch of paraffin sections were stained with safranin O/fast green, haematoxylin and eosin (H&E), or used for immunohistochemistry (IHC). Mankin Score⁶⁶ and Osteoarthritis Research Society International (OARSI) grade⁶⁷ were used to evaluate the severity and progress of OA after safranin-O and H&E staining. Factors affecting synovitis score included thickening of the whole synovial membrane, formation of lymphatic and aggregation of inflammatory cells⁶⁸ according to H&E-stained paraffin sections.

Frozen sections were reserved for immunohistochemistry-frozen. Slides were incubated with primary antibodies, such as rabbit anti-ADAMTS-5 (Abcam; ab41037), rabbit anti-MMP-13 (Abcam, ab75606), rabbit anti-LIF (Abcam, ab113262), rabbit anti-IL-6 (Abcam, ab179570), rabbit anti-CD14 (Abcam, ab221678) and rabbit anti-CD68 (Abcam, ab283654), overnight at 4°C, then the slides were incubated with Alexa Fluor 594-conjugated goat anti-Rabbit IgG (Abcam; ab150088) as the secondary antibody. Cell

nuclei were counterstained with DAPI. Finally, sections were scanned using a confocal microscope (Nikon, A1R), and fluorescence was analysed by preset pseudo colour.

MiR-27b-3p inhibition and overexpression, and preparation of target gene siRNA for in vitro assay

MiR-27b-3p mimic oligonucleotides, miR-27b-3p inhibitor oligonucleotides and negative control oligonucleotides (GenePharma Co. Ltd., Shanghai, China) were transfected into UCMSCs, mouse FLSs following the manufacturer's protocol. Small interfering RNA (siRNA) was used to deplete LIF. LIF siRNA (*siLIF*) sequences (GenePharma Co. Ltd., Shanghai, China) were also transfected into mouse FLSs according to the manufacturer's protocol. Briefly, the oligonucleotides were mixed with Lipofectamine 3000 Transfection Reagent (L3000001, Thermo Fisher Scientific) in Opti-MEM I reduced serum medium (Gibco, Thermo Fisher Scientific) and mixed gently without shaking. Culture medium was then replaced with this medium mixture (oligonucleotide concentration, 100 nM) and cells were then incubated for 24 h. The sequences are listed in Supporting Table S1.

Synthesis of target gene siRNA and in vivo assay

Chemically modified siRNA can be stably transfected into tissues and used for in vivo experiments.⁶⁹ Methoxy modified LIF siRNA (*m-siLIF*) and its negative control (*m-siLIF NC*) was synthesized by GenePharma Co. Ltd. (Shanghai, China). After DMM surgery, mice knee joints were injected by 6 μ l *m-siLIF* (0.5mg/mL) or *m-siLIF NC* twice a week. After 8 weeks, knee joints were harvested for histological analysis.

Luciferase reporter assay

To investigate whether LIF were downstream targets of miR-27b-3p by dual luciferase reporter gene assay, the biological prediction database microRNA.org was used. To construct the wild-type LIF 3'UTR-Luc reporter plasmid (LIF 3'UTR), the full length 3'UTRs of LIF, including the predicted miR-27b-3p binding site, were cloned, amplified, and introduced into the psi-CHECKTM-2 vector (Promega, Madison, WI, USA) downstream of the firefly luciferase gene using restriction enzyme sites XhoI and XbaI. After designing the mutation site of complementary sequences in the seed sequence on the LIF wild type (WT), the constructed luciferase reporter plasmids WT and mutant (MUT) were co-transfected with miR-27b-3p mimic and inhibitor into HEK-293T cells. After transfection for 48 h, luciferase activity was determined using a Dual-Glo luciferase assay system (Promega) according to the manufacturer's instructions.

RNA-seq library preparation and sequencing for single-cell RNA-sequencing (scRNA-seq)

Normal and OA patients' synovial tissues were disaggregated into single cell solutions with 100 μ g/mL of the enzyme mixture Liberase™ (Sigma-Aldrich) and 100 μ g/mL DNase I (New England Biolabs, Ipswich, MA, USA) as mentioned previously.⁷⁰ The resulting single-cell suspension was treated with RPMI-1640 medium to stop digestion and filtered through a cell strainer, then the 10 \times Chromium System was used

for single cell transcriptome isolation from a single cell solution which was kept on ice. Human synovial tissue was isolated from fracture and OA patient donors, obtained from the Department of Orthopaedics, Union Hospital, Tongji Medical College, Huazhong University of Science and Technology. The study was approved by the Union Hospital Ethical Committee and all patients provided their informed consent.

A single-cell RNA-Seq library kit v3 was used to prepare cells for cDNA amplification and chromium library construction according to the manufacturer's recommendations (10 × Genomics, Pleasanton, CA, USA) by the Wuhan Biobank Co., Ltd. cDNA libraries were sequenced on the Illumina NovaSeq 6,000 (Illumina Inc., San Diego, CA, USA) with a reading length of 150 bp.

Analysis of scRNA-seq data

The scRNA-seq data were primarily analysed following recommended protocols from 10× Genomics. Briefly, Illumina sequencer-generated raw base call (BCL) data were demultiplexed into FASTQ files, and alignment was carried out to the h19 human transcriptome on this basis. Cell Ranger software version 3.1 and default parameters (10× Genomics) were used to perform filtering, barcode counting, and unique molecular identifier (UMI) counting. The R package Seurat was used to perform secondary statistical analysis including quality control and subsequent analyses on the feature-barcode matrices which were produced by Cell Ranger. In Seurat, after basic filtering for minimum gene and cell observance frequency cut-offs, data were first normalised and scaled. The data were further examined and filtered (nFeature 6,000, nCount 10,000, percent_mt 0.25) according to a range of metrics in order to detect and exclude possible multiplets (i.e. instances where more than one cell was present and sequenced in a single emulsified gel bead). To reduce noise, regression methods were used for the removal of further technical artefacts.

After the quality control procedure was completed, linear dimensional reduction was performed to calculate the principal components using the genes with the most variable expression in the dataset. Seurat's FindNeighbors and FindClusters functions were used to group cells into an optimal number of clusters for new cell type discovery. We plotted Uniform Manifold Approximation and Projection (UMAP) to achieve graph-based clustering approaches with visualisation of cells, and reduced the information captured in the selected significant cardinal components to two dimensions. The particular cell type with differentially-expressed genes (DEGs), which were defined by a p value threshold < 0.05 and $\log FC > 0.25$, and provided p values were adjusted by Bonferroni correction.

RNA extraction and library preparation for mRNA sequencing (RNA-seq)

Total RNA was extracted from isolated mouse FLSs of vehicle- (serum-free human MSC expansion medium) and U-sEV- (1×10^8 particles per well) treated groups using TRIzol Reagent (Invitrogen) following the methods described in previous publications.⁷¹ DNA digestion was carried out after RNA extraction by DNase I. A Nanodrop™ OneC spectrophotometer (Thermo Fisher Scientific Inc.) was used to check RNA quality by reading the absorbance at A260/A280. RNA integrity was confirmed by 1.5%

agarose gel electrophoresis. A Qubit™ RNA Broad Range assay kit (Life Technologies, Thermo Fisher Scientific; Q10210) was used to finally quantify RNAs using the Qubit 3.0. An RNA sequencing library was prepared from 2 µg total RNA using a KCTM Stranded mRNA Library Prep Kit for Illumina® (Catalogue NO. DR08402, Wuhan Seqhealth Co., Ltd., Wuhan, China) according to the manufacturer's instructions. The 200–500 bps enriched PCR products was quantified and finally sequenced on a Novaseq 6000 sequencer (Illumina) model PE150.

RNA-Seq data analysis

We utilised Trimmomatic (version 0.36) to filter raw sequencing data, and then any low-quality reads acquired were discarded and the reads contaminated with adaptor sequences were trimmed. Reads mapped to the exon regions of each gene were counted using featureCounts (Subread-1.5.1; Bioconductor) and then reads per kilobase million (RPKMs) were calculated. The EdgeR package (version 3.12.1) was used to identify DEGs between groups. Differences in gene expression were considered statistically significant at a 0.05 cutoff *p*-value and 2-fold change. Gene ontology (GO) analysis, and Kyoto encyclopaedia of genes and genomes (KEGG) enrichment analysis for DEGs were both implemented by KOBAS software (version: 2.1.1). rMATS (version 3.2.5) was used to detect alternative splicing events with a false discovery rate (FDR) value cutoff of 0.05 and an absolute value of $\Delta\psi$ of 0.05.

Immunofluorescence

FLSs were seeded onto different concentrations of N-arachidonyldopamine (NADA; Abcam; ab120099) pre-treated slides and incubated at 37°C for 10 min. After fixation with 4% formaldehyde for 10 min at room temperature, cells were stained with rabbit anti-LIF (Abcam, ab113262) and rabbit anti-IL6 (Abcam, ab179570) overnight at 4°C, then Alexa Fluor 594-conjugated goat anti-Rabbit IgG (Abcam; ab150088) was used as the secondary antibody. FLS nuclei were finally stained with DAPI. A confocal microscope (Nikon, A1R) was used to scan the sections.

Micro-CT analysis

Mouse knee joints were harvested 8 weeks after DMM surgery and fixed in 4% paraformaldehyde for 48 h. Then, samples were scanned using a SkyScan 1176 high-resolution micro-CT imaging system (Bruker, Corp., Billerica, MA, USA) at 9 µm resolution with a 1 mm aluminium filter at a voltage of 90 kV and current of 273 µA. NRecon and CT-analyser software provided by SkyScan were used for volumetric reconstruction and analysis. The grade of OA progression and bone mineral density (bone volume/total volume, BV/TV) were analysed based on the micro-CT images.^{72,73}

Transwell assay

FLSs (5×10^6 /mL in 600 µL medium) were seeded into wells of a 24-well plate and incubated at 37°C for 2 h until cells had attached. After induction with 5 ng/mL IL-1β for 24 h, FLSs were transfected with siLIF. Meanwhile, after induction with 10 ng/mL rhLIF for 24 h, FLSs were incubated with U-sEV^{NC} or incubated with U-sEV^{miR-27b-3p}, as appropriate. Transwell filters (Costar, Dow Corning Corp., Midland, MI, USA) with

8 µm pore size were installed into wells and 5×10^3 RAW 264.7 macrophages in 150 µL growth medium were seeded into every filter. After 12 h of incubation, macrophages in the upper chamber of the filter were removed using a swab. Macrophages on the lower side of the filter were fixed and stained with crystal violet. The stained cells were considered to have migrated in response to the influence of FLSs in the lower chamber. The migrated macrophages were observed and quantified under an optical microscope. Each migration test group contained three independent wells.

OA pain analysis

Mouse knee pain was measured using von Frey fibres at 0, 4, 8 and 12 weeks after DMM surgery as described previously.⁷⁴ Every mouse was accustomed to an individual behavioural cubicle (4 × 3 × 7 cm) on a wire mesh grid (Shanghai Yuyan Instruments Co., Ltd., Shanghai, China) for 2 days prior to von Frey fibre testing. Before the test, mice were habituated to the cubicles for 20 minutes. Von Frey fibres 20 (Shanghai Yuyan Instruments Co., Ltd., Shanghai, China) ranging from 0.008 to 300 g were used for this assay. Each fibre was applied to the plantar surface of the rear paw until the fibre bent for 3 s. According to the 'top-down method',⁷⁵ X indicates a withdrawal response and O indicates no response. The formula shows that the threshold force eliciting paw withdrawal was represented as the 50% paw withdrawal threshold: $(10^{[X_r + k\delta]})/10,000$ (X_r = value of last von Frey filament used in the sequence (in log units), k = tabular value, and δ = mean difference in forces between fibres).⁷⁵

Real-time polymerase chain reaction (RT-PCR)

To calculate gene expression level, total RNA was isolated from cells using TRIzol (Invitrogen) according to the manufacturer's protocol. A high-capacity cDNA Reverse Transcription Kit (Applied Biosystems, Foster City, CA, USA) was used to reverse transcribe mRNA into cDNA. A Power SYBR Green PCR Master Mix Kit (Applied Biosystems) was used to perform quantitative real-time PCR. All primer sequences were designed using Primer 5.0 software, and sample differences were normalised to β -actin which was used as the internal reference. The relative expression level of genes was calculated using the $2^{-\Delta\Delta CT}$ method. The primer sequences used in this study are listed in Supporting Table S2.

Western blotting

Total protein was extracted from cells using RIPA lysis buffer (Thermo Fisher Scientific) and the concentration was quantified using a BCA kit (Sigma-Aldrich). Microsomal protein was then subjected to SDS-polyacrylamide gel electrophoresis under reducing conditions for 60 min and blotted onto a 0.45 µm polyvinylidene difluoride membrane for 60 min. Next, the membranes were immersed in bovine serum albumin overnight. After washing with PBS containing 0.01% Tween 20 (PBST) three times, membranes were then incubated with primary antibodies (all diluted 1:500): anti-IL-6 antibody (Abcam, ab179570), anti-LIF antibody (Abcam, ab113262), anti-CXCL1 antibody (Abcam, ab86436), anti-CCL3 antibody (Abcam, ab259372), anti-MMP-1 antibody (Abcam, ab137332), anti-Calnexin antibody (Abcam, ab92573), anti-ALIX antibody (Abcam, ab275377), anti-CD63 antibody (Abcam, ab134045), anti-CD81 antibody (Abcam, ab79559) and anti-CD9 antibody (Abcam, ab236630) at 4°C overnight. Glyceraldehyde 3-phosphate dehydrogenase (GAPDH, 1:200, Santa Cruz Biotechnology, Santa Cruz, CA, USA) was used as

an internal reference. Signals on the membrane were detected by electrochemiluminescence (ECL, Pierce, Rockford, IL, USA), and the protein band density of immune complexes was analysed using AlphaEaseFC (Alpha Innotech) software.

Statistical analysis

The summary graphical data are expressed as means \pm standard error of the mean (SEM). Two groups were compared via a two-tailed *t*-test. An ordinary one-way analysis of variances (ANOVA) was used for comparison among three or more groups, and two-way ANOVA was used for comparison between two factors within multiple groups. All data were analyzed using SPSS software 17.0 or GraphPad PRISM 8 (GraphPad Software Inc., La Jolla, CA, USA), and values of $p < 0.05$ denote statistical significance.

Declarations

ACKNOWLEDGMENTS

We wish to thank Xiao Lv (Department of Orthopaedics, Union Hospital, Tongji Medical College, Huazhong University of Science and Technology) and Ling Qing (Department of Orthopaedic Surgery, Perelman School of Medicine, University of Pennsylvania) for constructive comments on the manuscript and helpful discussion. We thank Wuhan Hamilton Biotechnology Co., Ltd. for providing UCMSCs and GMP facility.

The authors gratefully acknowledge the support of the National Natural Science Foundation of China (No. 82072509, 81672235), Wuhan Science and Technology Bureau (No. 2019020701011479) and Research Fund of Shanghai Municipal Health Commission for Clinical Research in Medical Science (Grant No. 202040084).

AUTHOR CONTRIBUTIONS

X. Z., W. C. and S. L. contributed equally to this work. **X. Z. and W. T.** designed the study. **H. T and W. T.** conceived this project. **X. Z., W. T., W. C. and S. L.** analyzed the data and co-wrote the paper. **X. Z., Y. H., H. P., Z. H., Z. W., Q. M. and F. Z.** performed in vitro and in vivo experiments, and analyzed the data. **Z. D., Y. W., Z. S., Y. L. and S. Y.** provided important experimental insights. All authors contributed to discussions during the entire paper.

Competing interests

The authors declare no competing interests.

References

1. T.W. O'Neill, P.S. McCabe and J. McBeth, Update on the epidemiology, risk factors and disease outcomes of osteoarthritis. *Best. Pract. Res. Clin. Rheumatol.* **32**, 312–326 (2018).

2. L. Sharma, Osteoarthritis of the Knee. *N. Engl. J. Med.* **384**, 51–59 (2021).
3. A. Mathiessen and P.G. Conaghan, Synovitis in osteoarthritis: current understanding with therapeutic implications. *Arthritis Res. Ther.* **19**, 18 (2017).
4. I. Atukorala, C.K. Kwok, A. Guermazi, F.W. Roemer, R.M. Boudreau, et al., Synovitis in knee osteoarthritis: a precursor of disease? *Ann. Rheum. Dis.* **75**, 390–5 (2016).
5. L. Liao, S. Zhang, L. Zhao, X. Chang, L. Han, et al., Acute Synovitis after Trauma Precedes and is Associated with Osteoarthritis Onset and Progression. *Int. J. Biol. Sci.* **16**, 970–980 (2020).
6. C. Manferdini, F. Paoletta, E. Gabusi, Y. Silvestri, L. Gambari, et al., From osteoarthritic synovium to synovial-derived cells characterization: synovial macrophages are key effector cells. *Arthritis Res. Ther.* **18**, 83 (2016).
7. B. Bartok and G.S. Firestein, Fibroblast-like synoviocytes: key effector cells in rheumatoid arthritis. *Immunol. Rev.* **233**, 233–55 (2010).
8. P.K. Gupta, A.K. Das, A. Chullikana and A.S. Majumdar, Mesenchymal stem cells for cartilage repair in osteoarthritis. *Stem Cell Res. Ther.* **3**, 25 (2012).
9. T.S. de Windt, L.A. Vonk, I.C. Slaper-Cortenbach, M.P. van den Broek, R. Nizak, et al., Allogeneic Mesenchymal Stem Cells Stimulate Cartilage Regeneration and Are Safe for Single-Stage Cartilage Repair in Humans upon Mixture with Recycled Autologous Chondrons. *Stem Cells* **35**, 256–264 (2017).
10. W. Tong, X. Zhang, Q. Zhang, J. Fang, Y. Liu, et al., Multiple umbilical cord-derived MSCs administrations attenuate rat osteoarthritis progression via preserving articular cartilage superficial layer cells and inhibiting synovitis. *J. Orthop. Translat.* **23**, 21–28 (2020).
11. X. Zhang, S. Liu, Z. Wang, C. Luo, Z. Dai, et al., Implanted 3D gelatin microcryogel enables low-dose cell therapy for osteoarthritis by preserving the viability and function of umbilical cord MSCs. *Chem. Eng. J.* **416**, 129140 (2021).
12. R.C. Lai, R.W. Yeo and S.K. Lim, Mesenchymal stem cell exosomes. *Semin. Cell Dev. Biol.* **40**, 82–8 (2015).
13. Q. Li, Y. Xu, K. Lv, Y. Wang, Z. Zhong, et al., Small extracellular vesicles containing miR-486-5p promote angiogenesis after myocardial infarction in mice and nonhuman primates. *Sci. Transl. Med.* **13**, (2021).
14. C.Y. Tan, R.C. Lai, W. Wong, Y.Y. Dan, S.K. Lim, et al., Mesenchymal stem cell-derived exosomes promote hepatic regeneration in drug-induced liver injury models. *Stem Cell Res. Ther.* **5**, 76 (2014).
15. J. Burrello, S. Monticone, C. Gai, Y. Gomez, S. Kholia, et al., Stem Cell-Derived Extracellular Vesicles and Immune-Modulation. *Front. Cell Dev. Biol.* **4**, 83 (2016).
16. C.M. Boulanger, X. Loyer, P.E. Rautou and N. Amabile, Extracellular vesicles in coronary artery disease. *Nat. Rev. Cardiol.* **14**, 259–272 (2017).
17. W.S. Toh, R.C. Lai, J.H.P. Hui and S.K. Lim, MSC exosome as a cell-free MSC therapy for cartilage regeneration: Implications for osteoarthritis treatment. *Semin. Cell Dev. Biol.* **67**, 56–64 (2017).

18. S. Kourembanas, Exosomes: vehicles of intercellular signaling, biomarkers, and vectors of cell therapy. *Annu. Rev. Physiol.* **77**, 13–27 (2015).
19. C.H. Woo, H.K. Kim, G.Y. Jung, Y.J. Jung, K.S. Lee, et al., Small extracellular vesicles from human adipose-derived stem cells attenuate cartilage degeneration. *J. Extracell. Vesicles* **9**, 1735249 (2020).
20. R. Yañez, M.L. Lamana, J. García-Castro, I. Colmenero, M. Ramírez, et al., Adipose tissue-derived mesenchymal stem cells have in vivo immunosuppressive properties applicable for the control of the graft-versus-host disease. *Stem Cells* **24**, 2582–91 (2006).
21. M. ter Huurne, R. Schelbergen, R. Blattes, A. Blom, W. de Munter, et al., Antiinflammatory and chondroprotective effects of intraarticular injection of adipose-derived stem cells in experimental osteoarthritis. *Arthritis Rheum.* **64**, 3604–13 (2012).
22. F. Djouad, C. Bouffi, S. Ghannam, D. Noël and C. Jorgensen, Mesenchymal stem cells: innovative therapeutic tools for rheumatic diseases. *Nat. Rev. Rheumatol.* **5**, 392–9 (2009).
23. Y. Liu, J. Fang, Q. Zhang, X. Zhang, Y. Cao, et al., Wnt10b-overexpressing umbilical cord mesenchymal stem cells promote critical size rat calvarial defect healing by enhanced osteogenesis and VEGF-mediated angiogenesis. *J. Orthop. Translat.* **23**, 29–37 (2020).
24. C. Théry, K.W. Witwer, E. Aikawa, M.J. Alcaraz, J.D. Anderson, et al., Minimal information for studies of extracellular vesicles 2018 (MISEV2018): a position statement of the International Society for Extracellular Vesicles and update of the MISEV2014 guidelines. *J. Extracell. Vesicles* **7**, 1535750 (2018).
25. H.N. Nguyen, E.H. Noss, F. Mizoguchi, C. Huppertz, K.S. Wei, et al., Autocrine Loop Involving IL-6 Family Member LIF, LIF Receptor, and STAT4 Drives Sustained Fibroblast Production of Inflammatory Mediators. *Immunity* **46**, 220–232 (2017).
26. P.I. Mapp and D.A. Walsh, Mechanisms and targets of angiogenesis and nerve growth in osteoarthritis. *Nat. Rev. Rheumatol.* **8**, 390–8 (2012).
27. V. Krenn, L. Morawietz, T. Haupl, J. Neidel, I. Petersen, et al., Grading of chronic synovitis—a histopathological grading system for molecular and diagnostic pathology. *Pathol. Res. Pract.* **198**, 317–25 (2002).
28. J. Phan, P. Kumar, D. Hao, K. Gao, D. Farmer, et al., Engineering mesenchymal stem cells to improve their exosome efficacy and yield for cell-free therapy. *J. Extracell. Vesicles* **7**, 1522236 (2018).
29. D. Riemann, G.H. Hansen, L. Niels-Christiansen, E. Thorsen, L. Immerdal, et al., Caveolae/lipid rafts in fibroblast-like synoviocytes: ectopeptidase-rich membrane microdomains. *Biochem. J.* **354**, 47–55 (2001).
30. L.A. Mulcahy, R.C. Pink and D.R. Carter, Routes and mechanisms of extracellular vesicle uptake. *J. Extracell. Vesicles* **3**, (2014).
31. S.E. Henrich, K.M. McMahon, M.P. Plebanek, A.E. Calvert, T.J. Feliciano, et al., Prostate cancer extracellular vesicles mediate intercellular communication with bone marrow cells and promote metastasis in a cholesterol-dependent manner. *J. Extracell. Vesicles* **10**, e12042 (2020).

32. R. Upadhyaya, L.N. Madhu, S. Attaluri, D.L.G. Gitaí, M.R. Pinson, et al., Extracellular vesicles from human iPSC-derived neural stem cells: miRNA and protein signatures, and anti-inflammatory and neurogenic properties. *J. Extracell. Vesicles* **9**, 1809064 (2020).
33. K. Khalaj, R.L. Figueira, L. Antounians, G. Lauriti and A. Zani, Systematic review of extracellular vesicle-based treatments for lung injury: are EVs a potential therapy for COVID-19? *J. Extracell. Vesicles* **9**, 1795365 (2020).
34. S. Öztürk, A.E. Elçin, A. Koca and Y.M. Elçin, Therapeutic Applications of Stem Cells and Extracellular Vesicles in Emergency Care: Futuristic Perspectives. *Stem Cell Rev. Rep.* **17**, 390–410 (2021).
35. Y. Luo, D. Gao, P. Wang, C. Lou, T. Li, et al., Optimized culture methods for isolating small extracellular vesicles derived from human induced pluripotent stem cells. *J. Extracell. Vesicles* **10**, e12065 (2021).
36. C. Lechanteur, A. Briquet, V. Bettonville, E. Baudoux and Y. Beguin, MSC Manufacturing for Academic Clinical Trials: From a Clinical-Grade to a Full GMP-Compliant Process. *Cells* **10**, (2021).
37. K. O'Brien, K. Breyne, S. Ughetto, L.C. Laurent and X.O. Breakefield, RNA delivery by extracellular vesicles in mammalian cells and its applications. *Nat. Rev. Mol. Cell Biol.* **21**, 585–606 (2020).
38. S. Chand, A. Gowen, M. Savine, D. Moore, A. Clark, et al., A comprehensive study to delineate the role of an extracellular vesicle-associated microRNA-29a in chronic methamphetamine use disorder. *J. Extracell. Vesicles* **10**, e12177 (2021).
39. K. Yamana, J. Inoue, R. Yoshida, J. Sakata, H. Nakashima, et al., Extracellular vesicles derived from radioresistant oral squamous cell carcinoma cells contribute to the acquisition of radioresistance via the miR-503-3p-BAK axis. *J. Extracell. Vesicles* **10**, e12169 (2021).
40. J. Wu, L. Kuang, C. Chen, J. Yang, W.N. Zeng, et al., miR-100-5p-abundant exosomes derived from infrapatellar fat pad MSCs protect articular cartilage and ameliorate gait abnormalities via inhibition of mTOR in osteoarthritis. *Biomaterials* **206**, 87–100 (2019).
41. Z. Jin, J. Ren and S. Qi, Human bone mesenchymal stem cells-derived exosomes overexpressing microRNA-26a-5p alleviate osteoarthritis via down-regulation of PTGS2. *Int. Immunopharmacol.* **78**, 105946 (2020).
42. D. Kang, J. Shin, Y. Cho, H.S. Kim, Y.R. Gu, et al., Stress-activated miR-204 governs senescent phenotypes of chondrocytes to promote osteoarthritis development. *Sci. Transl. Med.* **11**, (2019).
43. J. Huang, L. Zhao, Y. Fan, L. Liao, P.X. Ma, et al., The microRNAs miR-204 and miR-211 maintain joint homeostasis and protect against osteoarthritis progression. *Nat. Commun.* **10**, 2876 (2019).
44. S. Miyaki and H. Asahara, Macro view of microRNA function in osteoarthritis. *Nat. Rev. Rheumatol.* **8**, 543–52 (2012).
45. S. Shen, Y. Wu, J. Chen, Z. Xie, K. Huang, et al., CircSERPINE2 protects against osteoarthritis by targeting miR-1271 and ETS-related gene. *Ann. Rheum. Dis.* **78**, 826–836 (2019).
46. R. Coutinho de Almeida, Y.F.M. Ramos, A. Mahfouz, W. den Hollander, N. Lakenberg, et al., RNA sequencing data integration reveals an miRNA interactome of osteoarthritis cartilage. *Ann. Rheum. Dis.* **78**, 270–277 (2019).

47. S. Jiang, G. Tian, Z. Yang, X. Gao, F. Wang, et al., Enhancement of acellular cartilage matrix scaffold by Wharton's jelly mesenchymal stem cell-derived exosomes to promote osteochondral regeneration. *Bioact. Mater.* **6**, 2711–2728 (2021).
48. L. Yan and X. Wu, Exosomes produced from 3D cultures of umbilical cord mesenchymal stem cells in a hollow-fiber bioreactor show improved osteochondral regeneration activity. *Cell Biol. Toxicol.* (2019).
49. X. Lu, Y. Yu, F. Yin, C. Yang, B. Li, et al., Knockdown of PVT1 inhibits IL-1 β -induced injury in chondrocytes by regulating miR-27b-3p/TRAF3 axis. *Int. Immunopharmacol.* **79**, 106052 (2020).
50. J.X. Yeh, K.L.W. Schultz, V. Calvert, E.F. Petricoin and D.E. Griffin, The NF- κ B/leukemia inhibitory factor/STAT3 signaling pathway in antibody-mediated suppression of Sindbis virus replication in neurons. *Proc. Natl. Acad. Sci. U S A* **117**, 29035–29045 (2020).
51. D.J. Hilton, LIF: lots of interesting functions. *Trends. Biochem. Sci.* **17**, 72–6 (1992).
52. N.A. Nicola and J.J. Babon, Leukemia inhibitory factor (LIF). *Cytokine Growth Factor Rev.* **26**, 533–44 (2015).
53. S.A. Jones and B.J. Jenkins, Recent insights into targeting the IL-6 cytokine family in inflammatory diseases and cancer. *Nat. Rev. Immunol.* **18**, 773–789 (2018).
54. B. Le Goff, S. Singbrant, B.A. Tonkin, T.J. Martin, E. Romas, et al., Oncostatin M acting via OSMR, augments the actions of IL-1 and TNF in synovial fibroblasts. *Cytokine* **68**, 101–9 (2014).
55. M. Lotz, T. Moats and P.M. Villiger, Leukemia inhibitory factor is expressed in cartilage and synovium and can contribute to the pathogenesis of arthritis. *J. Clin. Invest.* **90**, 888–96 (1992).
56. Y. Jiang, Q. Xiao, Z. Hu, B. Pu, J. Shu, et al., Tissue levels of leukemia inhibitory factor vary by osteoarthritis grade. *Orthopedics* **37**, e460-4 (2014).
57. G. Nygaard and G.S. Firestein, Restoring synovial homeostasis in rheumatoid arthritis by targeting fibroblast-like synoviocytes. *Nat. Rev. Rheumatol.* **16**, 316–333 (2020).
58. C.H. Chou, V. Jain, J. Gibson, D.E. Attarian, C.A. Haraden, et al., Synovial cell cross-talk with cartilage plays a major role in the pathogenesis of osteoarthritis. *Sci. Rep.* **10**, 10868 (2020).
59. A.P. Croft, J. Campos, K. Jansen, J.D. Turner, J. Marshall, et al., Distinct fibroblast subsets drive inflammation and damage in arthritis. *Nature* **570**, 246–251 (2019).
60. L. Danks, N. Komatsu, M.M. Guerrini, S. Sawa, M. Armaka, et al., RANKL expressed on synovial fibroblasts is primarily responsible for bone erosions during joint inflammation. *Ann. Rheum. Dis.* **75**, 1187–95 (2016).
61. R.J. Colman, Non-human primates as a model for aging. *Biochim. Biophys. Acta. Mol. Basis Dis.* **1864**, 2733–2741 (2018).
62. C. Thery, K.W. Witwer, E. Aikawa, M.J. Alcaraz, J.D. Anderson, et al., Minimal information for studies of extracellular vesicles 2018 (MISEV2018): a position statement of the International Society for Extracellular Vesicles and update of the MISEV2014 guidelines. *J. Extracell. Vesicles* **7**, 1535750 (2018).

63. S. Samavedi, P. Diaz-Rodriguez, J.D. Erndt-Marino and M.S. Hahn, A Three-Dimensional Chondrocyte-Macrophage Coculture System to Probe Inflammation in Experimental Osteoarthritis. *Tissue Eng. Part A* **23**, 101–114 (2017).
64. A.D. Lynn and S.J. Bryant, Phenotypic changes in bone marrow-derived murine macrophages cultured on PEG-based hydrogels activated or not by lipopolysaccharide. *Acta Biomater.* **7**, 123–32 (2011).
65. S.S. Glasson, T.J. Blanchet and E.A. Morris, The surgical destabilization of the medial meniscus (DMM) model of osteoarthritis in the 129/SvEv mouse. *Osteoarthritis Cartilage* **15**, 1061–9 (2007).
66. M.A. McNulty, R.F. Loeser, C. Davey, M.F. Callahan, C.M. Ferguson, et al., Histopathology of naturally occurring and surgically induced osteoarthritis in mice. *Osteoarthritis Cartilage* **20**, 949–56 (2012).
67. S.S. Glasson, M.G. Chambers, W.B. Van Den Berg and C.B. Little, The OARSI histopathology initiative - recommendations for histological assessments of osteoarthritis in the mouse. *Osteoarthritis Cartilage* **18 Suppl 3**, S17-23 (2010).
68. L. Haywood, D.F. McWilliams, C.I. Pearson, S.E. Gill, A. Ganesan, et al., Inflammation and angiogenesis in osteoarthritis. *Arthritis Rheum.* **48**, 2173–7 (2003).
69. W.F. Lima, T.P. Prakash, H.M. Murray, G.A. Kinberger, W. Li, et al., Single-stranded siRNAs activate RNAi in animals. *Cell* **150**, 883–94 (2012).
70. F. Zhang, K. Wei, K. Slowikowski, C.Y. Fonseka, D.A. Rao, et al., Defining inflammatory cell states in rheumatoid arthritis joint synovial tissues by integrating single-cell transcriptomics and mass cytometry. *Nat. Immunol.* **20**, 928–942 (2019).
71. P. Chomczynski and N. Sacchi, Single-step method of RNA isolation by acid guanidinium thiocyanate-phenol-chloroform extraction. *Anal. Biochem.* **162**, 156–9 (1987).
72. J.E. Kim, S.M. Lee, S.H. Kim, P. Tatman, A.O. Gee, et al., Effect of self-assembled peptide-mesenchymal stem cell complex on the progression of osteoarthritis in a rat model. *Int. J. Nanomedicine* **9 Suppl 1**, 141–57 (2014).
73. W.P. Chan, P. Lang, M.P. Stevens, K. Sack, S. Majumdar, et al., Osteoarthritis of the knee: comparison of radiography, CT, and MR imaging to assess extent and severity. *AJR Am. J. Roentgenol.* **157**, 799–806 (1991).
74. M.J. Piel, J.S. Kroin and H.J. Im, Assessment of knee joint pain in experimental rodent models of osteoarthritis. *Methods Mol. Biol.* **1226**, 175–81 (2015).
75. S.R. Chaplan, F.W. Bach, J.W. Pogrel, J.M. Chung and T.L. Yaksh, Quantitative assessment of tactile allodynia in the rat paw. *J. Neurosci. Methods* **53**, 55–63 (1994).

Figures

Figure 1

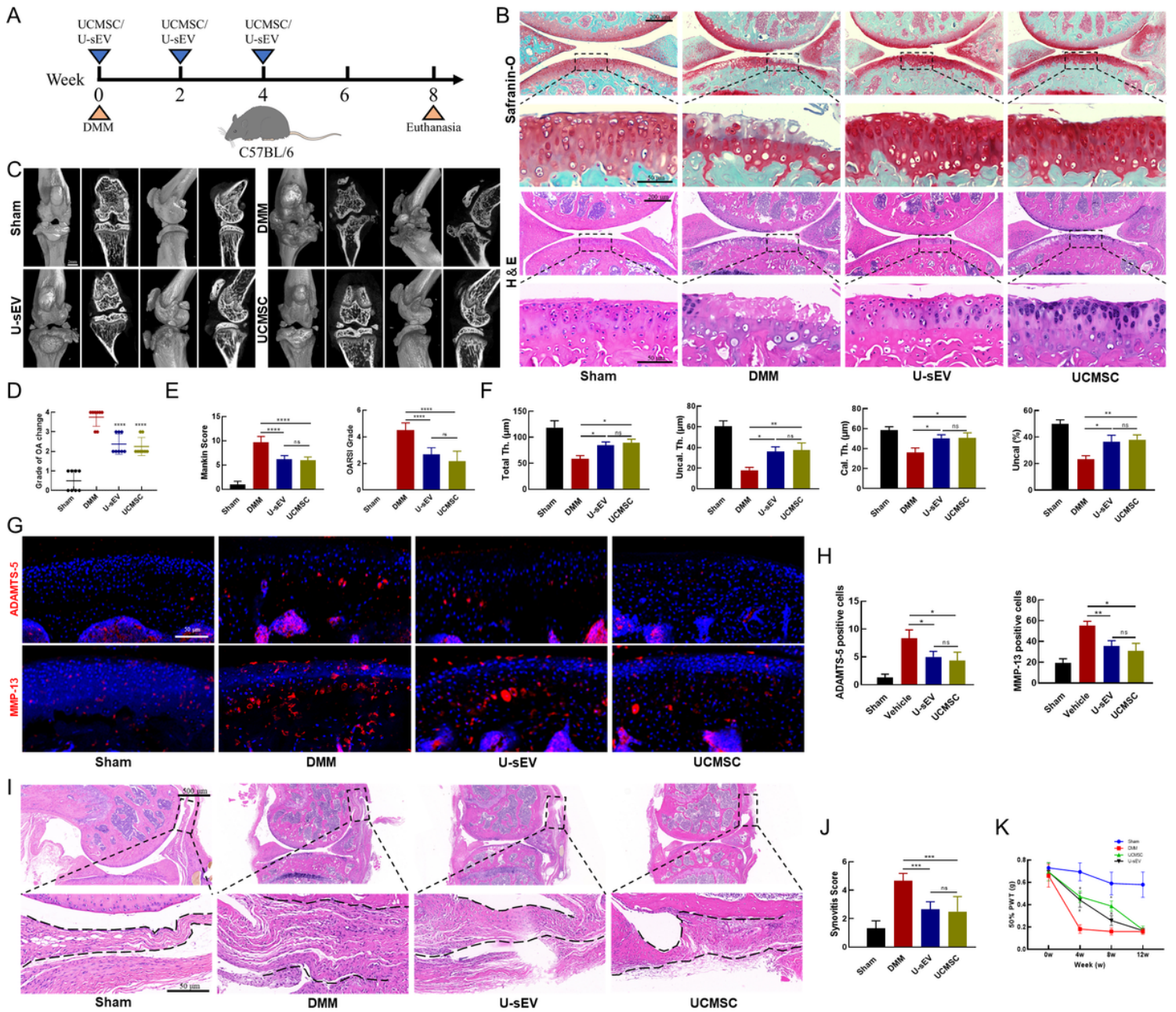


Figure 1

U-sEVs exhibited similar effects to delay OA progression as UCMSCs did. (A) Schematic showing the study protocol of C57BL/6 mice with DMM surgery, followed by UCMSC and U-sEV injection 0, 2, 4 weeks after surgery. (B) Safranin O/Fast green and H&E staining of sham-operated joints, DMM, U-sEV and UCMSC injection into a DMM induced mouse model of knee OA. (C) Representative images of anterior and medial views of the knee joint in all groups by micro-CT analysis at 8th week after injection. (D) The grade of OA change of individual samples in all groups. $n = 8$. (E) Mankin score and OARSI grade for measuring the OA severity. $n = 8$. (F) Average thicknesses of total articular cartilage in tibial plateau (Total Th.), uncalcified (Uncal. Th.) cartilage, calcified (Cal) cartilage and percentage of uncalcified zone over the whole cartilage layer (Uncal (%)). $n = 8$. (G) Immunofluorescence staining of ADAMTS-5 and MMP-13

in knee joint sections of mice. (H) Quantification of ADAMTS-5⁺ and MMP-13⁺ cells in the fixed region. $n = 8$. (I) H&E staining showing the inflammatory cell infiltration and thickness of the synovium (dashed lines) in each group. (J) Quantification of synovitis score. $n = 8$. (K) Pain analysis by Von Frey assay according to paw withdrawal threshold (PWT) in weeks 0, 4, 8 and 12 after treatment with UCMSC or U-sEV treatment. $n = 8$. * $P < 0.05$, ** $P < 0.01$, *** $P < 0.001$, **** $P < 0.0001$. ns = not significant.

Figure 2

Uptake assay of U-sEV in vivo and in vitro. (A, B, C) DiO-labeled U-sEVs were injected into mouse knee joints. After 1, 3 and 7 days, knee sections were stained with DAPI and scanned by confocal microscopy. Synovium, cartilage and meniscus area were emphatically observed as regions of interest. (D, E, F) Fluorescence images detected internalization of U-sEV. DiO-labeled small extracellular vesicles (green) was were detected in the fibroblast-like synoviocytes (FLSs), CHOs and MFCs whose cytoskeleton were stained with phalloidin (red). FLS: fibroblast-like synoviocytes; CHO: chondrocyte; MFC: meniscus fibroblast chondrocyte. (G) Mean green fluorescent intensity (MFI) per cell was calculated accordingly. $n = 3$. & $P < 0.05$ vs. MFC (1h), ##### $P < 0.0001$ vs. CHO (2h).

Figure 3

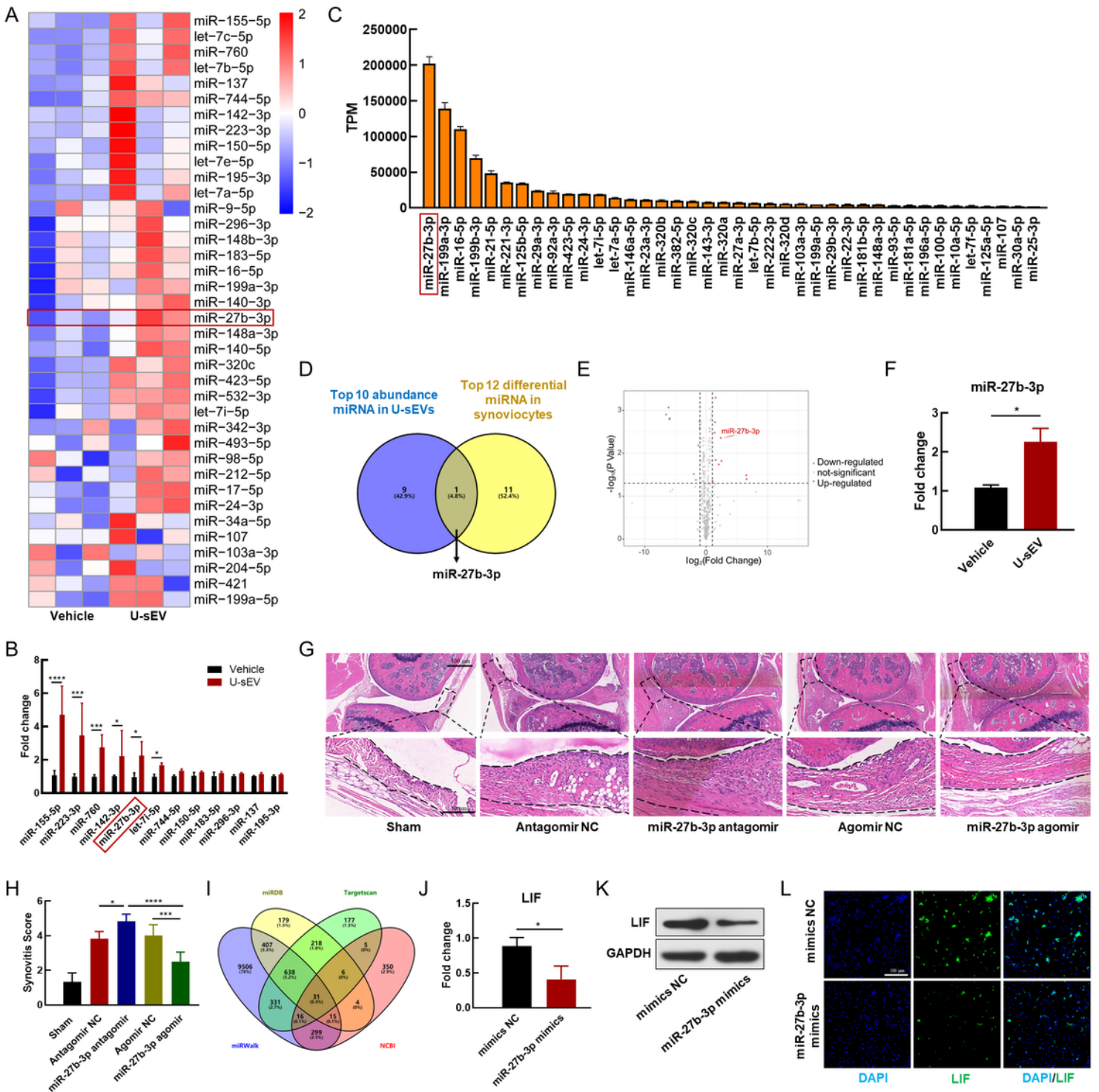


Figure 3

Analysis of miRNA and mRNA sequencing of U-sEVs treated mouse FLSs. (A) Heatmap analyzed increased miRNA in U-sEVs treated FLSs according to miRNA sequencing. $n = 3$. (B) miRNA abundance measured via RT-PCR in FLSs incubated with U-sEVs and vehicle and normalized to measurements in vehicle. $n = 3$. (C) Transcripts per million reads (TPM) in U-sEVs showed the top 40 high-abundance miRNAs according to miRNA sequencing. $n = 3$. (D) miR-27b-3p coexisted in top 10 abundance miRNA in

U-sEV and top 12 differential expressed miRNA in FLSs. $n = 3$. (E) Volcano blot showed that miR-27b-3p was significantly upregulated in U-sEV treated FLSs according to miRNA sequencing. $n = 3$. (F) RT-PCR assay demonstrated that the level of miR-27b-3p in FLSs was increased by U-sEV treatment. $n = 3$. (G) H&E staining showing the inflammatory cell infiltration and thickness of the synovium (dashed lines) in sham, antagomir NC, miR-27b-3p antagomir, agomir NC, and miR-27b-3p agomir group. (H) Quantification of synovitis score. $n = 6$. (I) Putative miR-27b-3p targets genes were identified using miRWalk, miRDB and Targetscan, and 31 genes were identified as miR-27b-3p target genes. (J, K) Transfection of miR-27b-3p decrease the gene expression of LIF in FLSs according to RT-PCR and western blotting assay. $n = 3$. (L) Immunofluorescence showed that cytoplasmic protein of LIF (green) was decreased expressed in FLSs by transfection of miR-27b-3p compared with vehicle. $*P < 0.05$, $***P < 0.001$, $****P < 0.0001$.

Figure 4

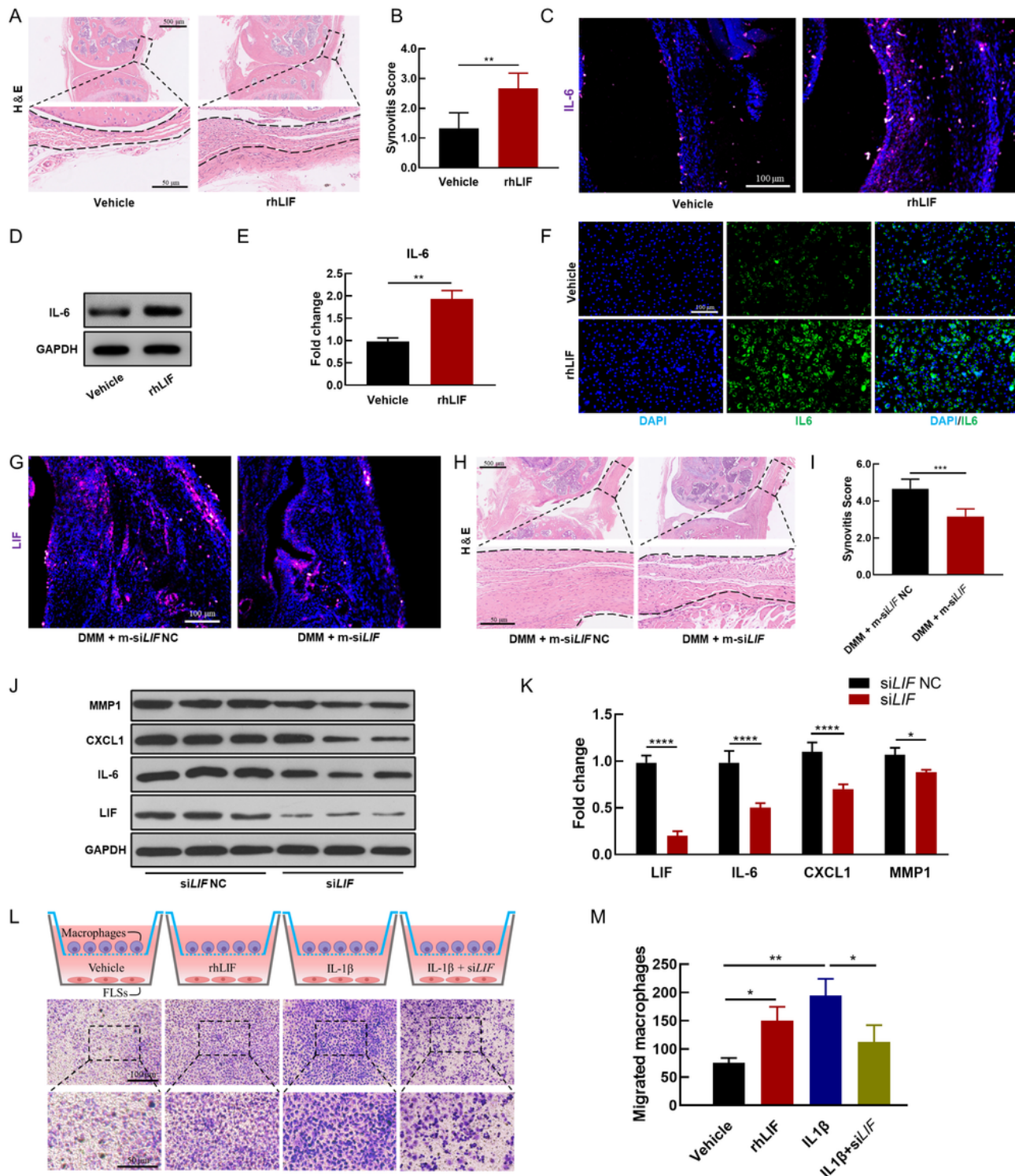


Figure 4

The proinflammatory effect of LIF in synovitis. (A) H&E staining showing the inflammatory cell infiltration and thickness of the synovium (dashed lines) in each group. (B) Quantification of synovitis score. $n = 8$. (C) Immunofluorescence staining of IL-6 on mouse synovium in knee joint sections of mice. (D, E) The expression of IL-6 in FLSs was analyzed using western blotting and RT-PCR assay. $n = 3$. (F) Immunofluorescence showed that cytoplasmic protein of IL-6 (green) was increased expressed in FLSs

by rhLIF treatment compared with vehicle. (G) Immunofluorescence staining of LIF on mouse synovium. (H) H&E staining of DMM + m-siLIF NC and DMM + m-siLIF treated mouse synovium. (I) Quantification of synovitis score. (J, K) After FLSs were induced by IL-1 β , the expression level of MMP1, CXCL1, IL-6 and LIF in siLIF and siLIF^{NC} transfected FLSs were analyzed using western blotting and RT-PCR assay. $n = 3$. (L) Vehicle (DMEM) (first panel) or rhLIF treated (second panel) FLSs on the lower chamber for 24 hours, and then changed to DMEM, with macrophages on the upper chamber. Twelve hours later crystal violet staining was performed. Similarly, IL-1 β treated FLSs added siLIF NC (third panel) or siLIF (fourth panel) for 24 hours, and then changed to DMEM, with macrophages on the upper chamber. Twelve hours later crystal violet staining was performed to show migrated cells. (M) Quantification of migrated macrophages. $n = 3$. * $P < 0.05$, ** $P < 0.01$, *** $P < 0.001$, **** $P < 0.0001$. ns = not significant.

Figure 5

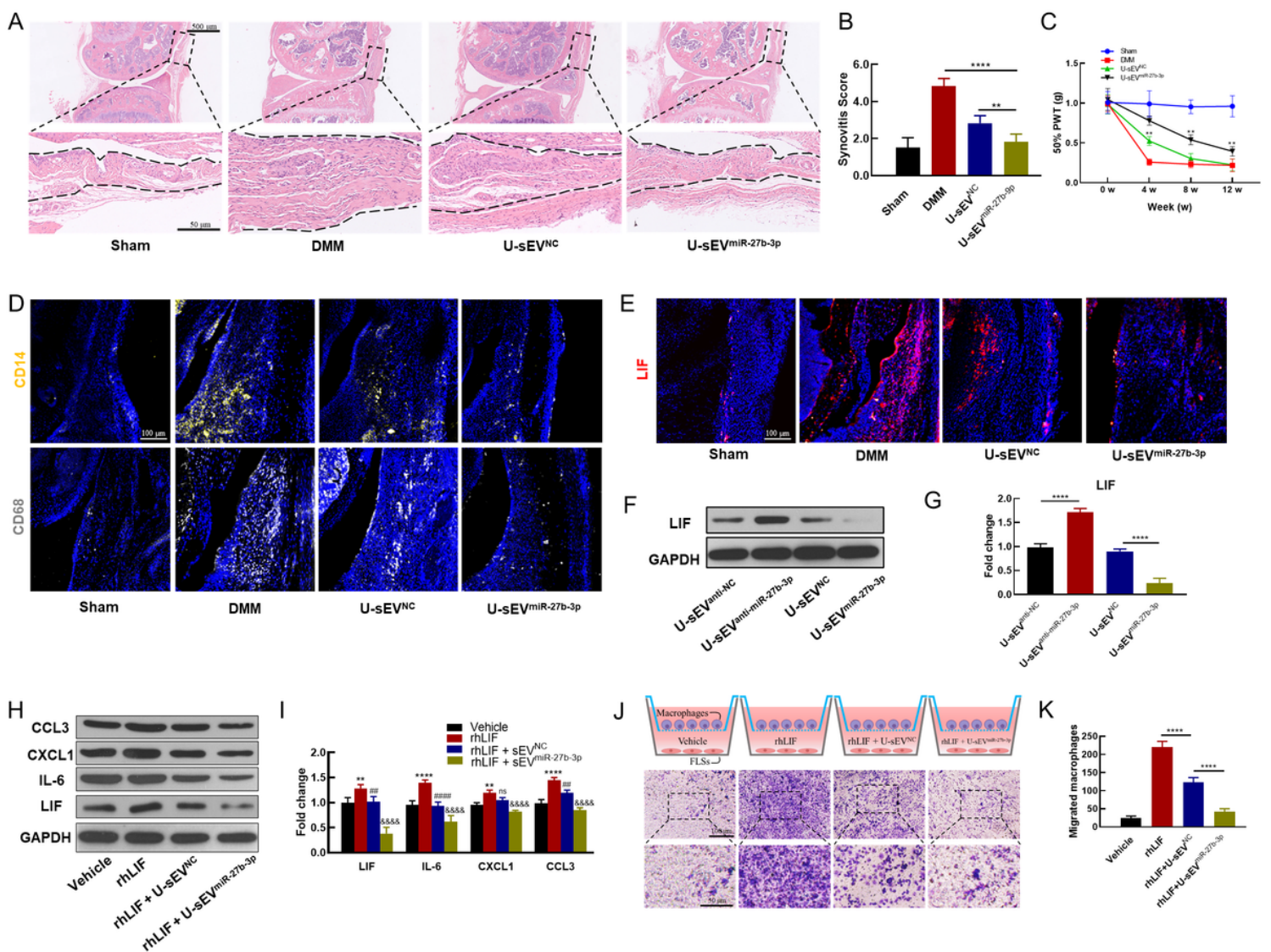


Figure 5

miR-27b-3p in U-sEVs mitigated synovitis by inhibiting LIF expression in FLS. (A) H&E staining showing the inflammatory cell infiltration and thickness of the synovium (dashed lines) in each group. (B)

Quantification of synovitis score. $n = 8$. (C) Pain analysis by Von Frey assay according to paw withdrawal threshold (PWT) at weeks 0, 4, 8 and 12 after treatment with U-sEV^{NC} or U-sEV^{miR-27b-3p} treatment. $n = 8$. (D) Immunofluorescence staining of CD14 and CD68 in knee joint sections of mice. (E) Immunofluorescence staining of LIF in knee joint sections of mice. (F, G) The expression of LIF in FLSs were analyzed using western blotting and RT-PCR assay. $n = 3$. (H, I) The expression level of CCL3, CXCL1, IL-6 and LIF in U-sEV^{NC} and U-sEV^{miR-27b-3p} treated FLSs which were induced by rhLIF were analyzed using western blotting and RT-PCR assay, $n = 3$. $**P < 0.01$ vs. Vehicle, $##P < 0.01$ and $####P < 0.0001$ vs. rhLIF, $#####P < 0.0001$ vs. rhLIF + U-sEV^{NC}. (J) Vehicle (DMEM) (first panel) or rhLIF treated FLSs along with U-sEV^{NC} (third panel) or U-sEV^{miR-27b-3p} (fourth panel) on the lower chamber for 24 hours, and then changed to DMEM, with macrophages seeded on the upper chamber. Twelve hours later crystal violet staining was performed to show migrated cells. (K) Quantification of migrated macrophages. $n = 3$. $*P < 0.05$, $**P < 0.01$, $***P < 0.001$, $****P < 0.0001$. ns = not significant.

Figure 6

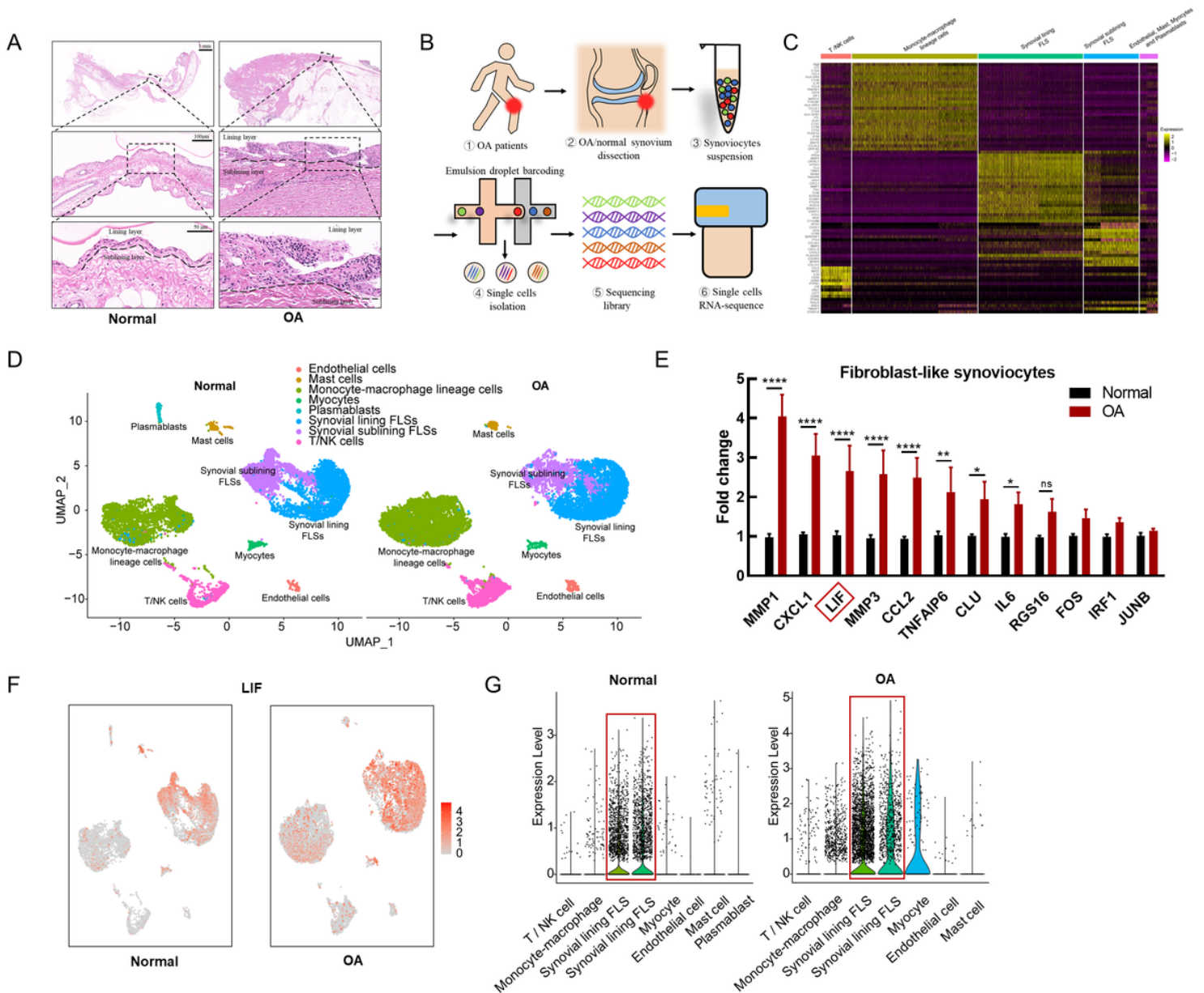


Figure 6

Difference between normal and OA synovium revealed by ScrRNA-seq. (A) H&E staining of synovium from normal and OA patients. (B) Schematic workflow of experimental strategy illustrated the preparation of cell populations. (C) Hierarchical single-cell transcriptional profiles clustering of cells into groups and scaled expression of differentially expressed genes for each cluster were showed by heatmap. (D) Visualization of UMAP colored pooled from cell clusters for human normal and OA synovium single-cell transcriptomes. (E) The most differentially expressed genes level in normal and OA synovium in fibroblast-like synoviocytes clusters were measured via RT-PCR and normalized to normal synovium group. (F) The cells are colored in UMAP map according to the expression levels of various genes. (G) The expression levels of various genes in cell clusters in normal and OA synovium were showed by violin plots image. * $P < 0.05$, ** $P < 0.01$, **** $P < 0.0001$. ns = not significant.

Figure 7

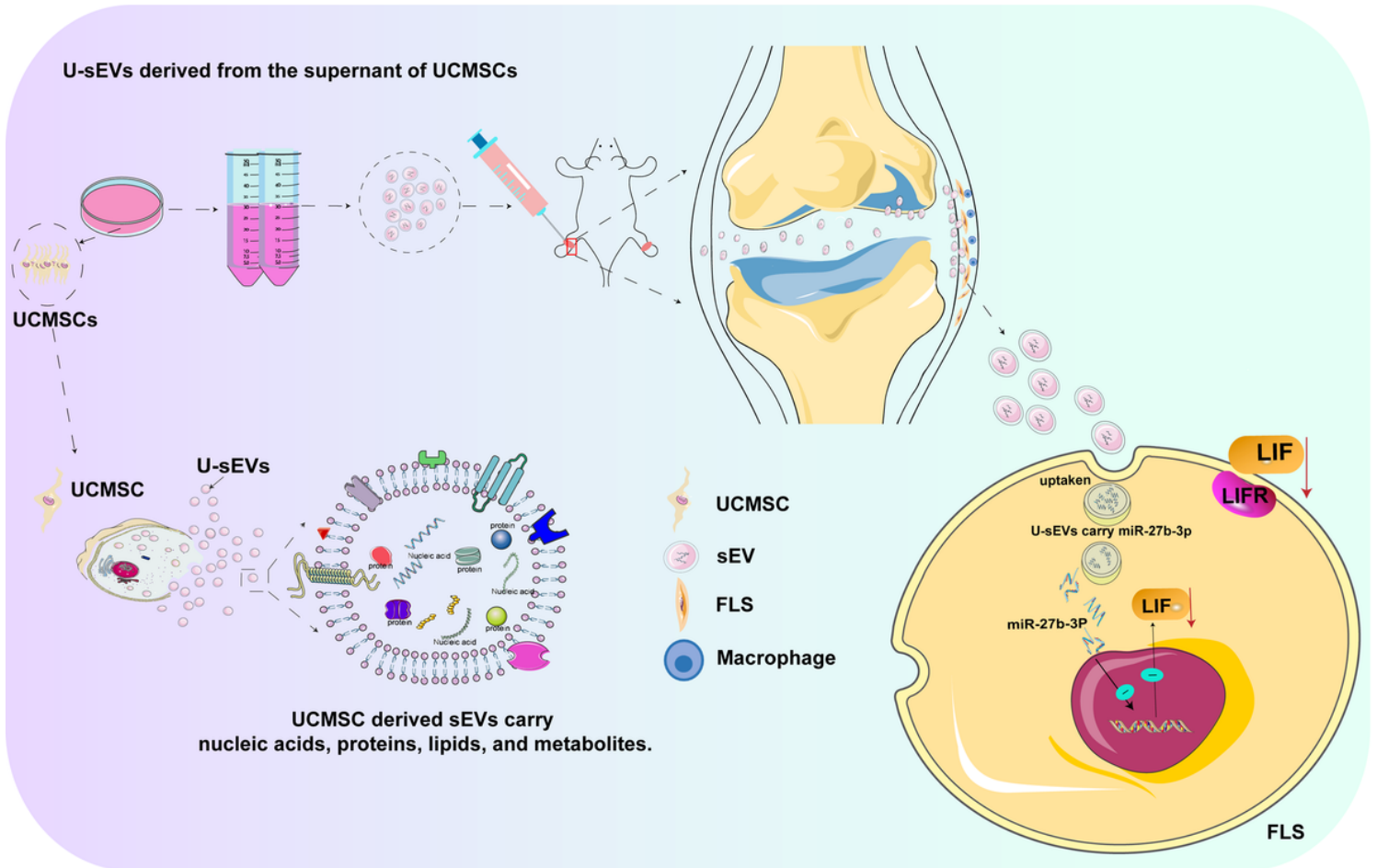


Figure 7

Schematic representation of the mechanism how U-sEVs containing miR-27b-3p mitigated OA.

Supplementary Files

This is a list of supplementary files associated with this preprint. Click to download.

- [SupportingInformation.docx](#)